Electronic Supplementary Information

A hybrid redox flow battery with high energy efficiency using low cost sandwiched membrane as separator and $LiMn_2O_4$ as cathode

Hanping Zhang,[a*] Shanshan Liang,[a] Baoping Sun,[b] Xiaojian Yang,[a] Xin Wu[a] and Tao Yang[a]

[a] Jiangsu Key Laboratory of advanced Catalytic materials and technology, Changzhou University, Changzhou 213164, China

[b] Shandong Vocational College of Economics and Business, Weifang, 261011, China

*E-mail: jinhongshi0001@163.com

Preparation of the hybrid redox flow battery (HRFB). The $LiMn_2O_4$ was prepared by solid-state reaction with a sucrose-assisted sol-gel method. 0.4 g starch was placed in a water-free flask and 25 mL distilled H_2O was added into the flask. The resultant mixture was heated initially at 110 °C until the solution become transparent under stirring (acted as solution A). Then 5 mmol manganese nitrate (50%) and 2.5 mmol lithium nitrate were added together and dissolved to get a homogeneous solution (acted as solution B). Solution B was added into solution A under stirring and then the mixture was kept at 110 °C for 1.5 h. The resultant mixture was dried initially at 110 °C to get the precursor in the form of foam. The dried foam was further heated at 250 °C for 3 h followed by a thermal treatment at 700 °C for 3 h to get $LiMn_2O_4$. The as-prepared $LiMn_2O_4$ was mixed with acetylene black and poly(tetrafluoroethylene) (PTFE) in a weight ratio of 7.5:1.5:1 with the help of ethanol. After drying, the mixture was pressed into a film, and then the film was cut into disks of about 1.5 mg and 0.4 cm^2. These disks were pressed onto a Ni-grid at a pressure of 10 MPa and then dried at 80 °C for one night to get disks with a thickness 100 um acting as the positive electrodes.

The negative side consists of Cr^{3+} aqueous solution, which was prepared by adding 1 mol L^{-1}

LiOH into 30 wt% $Cr_2(SO_4)_3$ acidic aqueous solution until deposits appear. Li_2SO_4 solution (15 wt%) was added into the solution as the supporting electrolyte. 10 ml of the solution was loaded in the negative side of the H-Shaped in-house model cell and was connected to a glass reservoir containing 50 mL anolytes. The solution was cycled by a peristaltic pump. The velocity can be modified to examine mass transport control. In this study, we use the flow rate (hence residence time) and electrolyte velocity at 20 mL min^{-1} (0.35 cm s^{-1} flow velocity).

The sandwiched membrane was prepared as follows: At first, a mixture of 0.1 mL 1 mol L^{-1} $LiClO_4$ and 2 g 5wt% PMMA (polymethylmethacrylate) in N-methyl-2-pyrrolidone (NMP) solution was cast on a porous PVDF (poly(vinylidene fluoride), Shanghai Beijia Chemical Co. Ltd.) film. The mass ratio of $LiClO_4$ and PMMA is about 1:10. After dried at 75 °C in vacuum for 18 h, another layer of the porous PVDF film was covered on the PMMA layer containing $LiClO_4$ salt. Then the membrane was tailored into a disk with a thickness of about 0.2 mm and an effective area of 0.5 cm^2.

The prepared electrodes and sandwiched membrane were assembled together and sealed with silicon grease.

Evaluation of the hybrid redox flow battery. The electrochemical tests were carried out at room temperature. All solutions were washed by N_2 flow for 10 minutes prior to tests. CV test was measured by using an electrochemical workstation (CHI660C, Shanghai) by using the $LiMn_2O_4$ as work electrode and the negative solution as the counter and reference electrode. The voltage of galvanostatic charge–discharge test (Fig. 2b and c) was between 0.5 and 1.5 V using a Lander cycler (Wuhan, China). Elemental analysis by inductively coupled plasma (Fig. 2c, ICP, Thermo

E. IRIS Duo) was performed by taking 1 mL solution at various voltages. The solution was then diluted 1000 times by adding water prior to the ICP test.

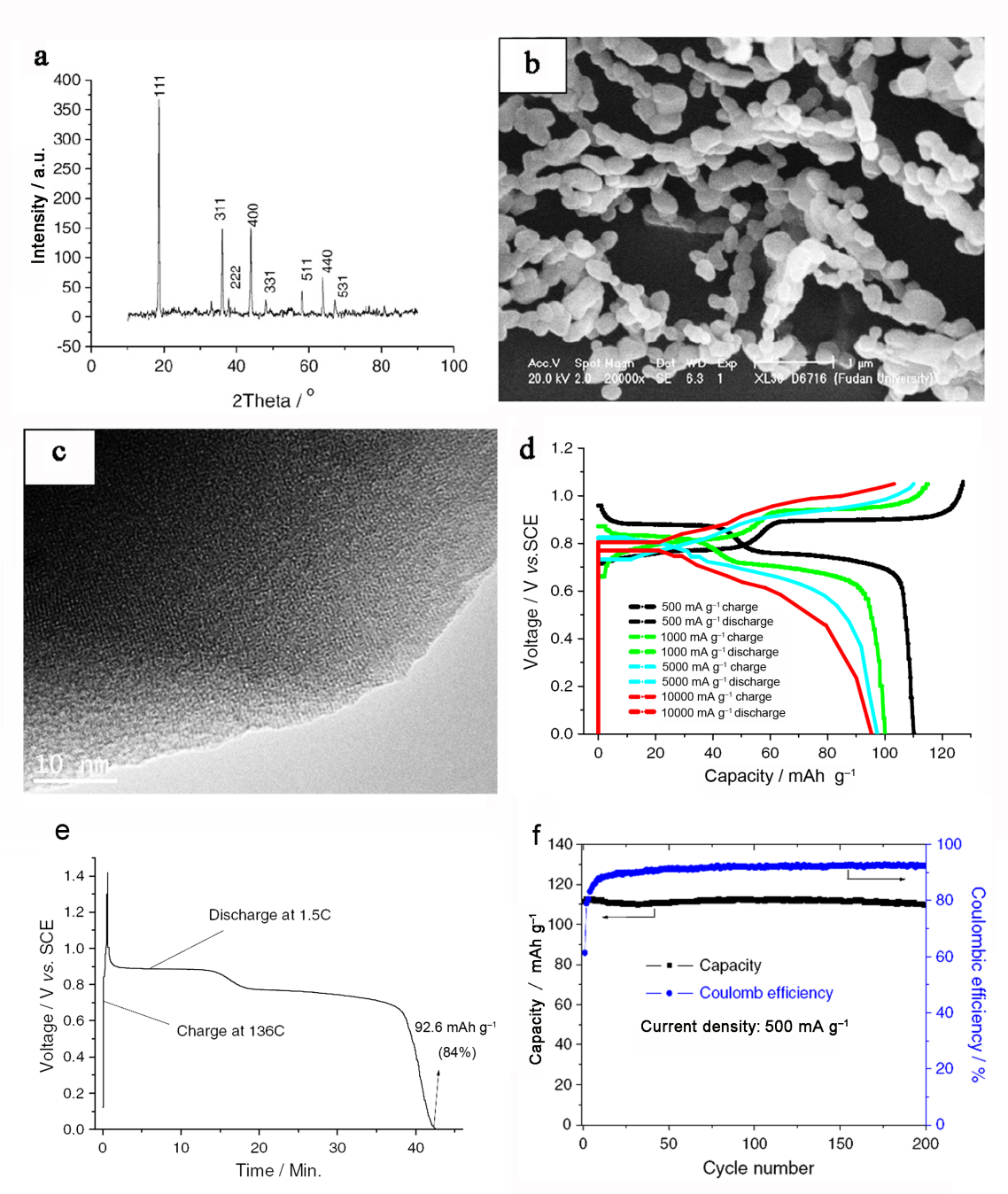

Fig. S1. Physical and electrochemical characterization of the as-prepared $LiMn_2O_4$ sample. (a) XRD, (b) SEM, (c) HRTEM, and (d) charge-discharge curves at various current densities, (e) reverse capacity at large charge density and (f) a further long-life test, cycling behaviour was performed at the current density of 500 mA h g^{-1} in 0.5 mol L^{-1} Li_2SO_4 aqueous electrolyte with the active carbon as the counter electrode.

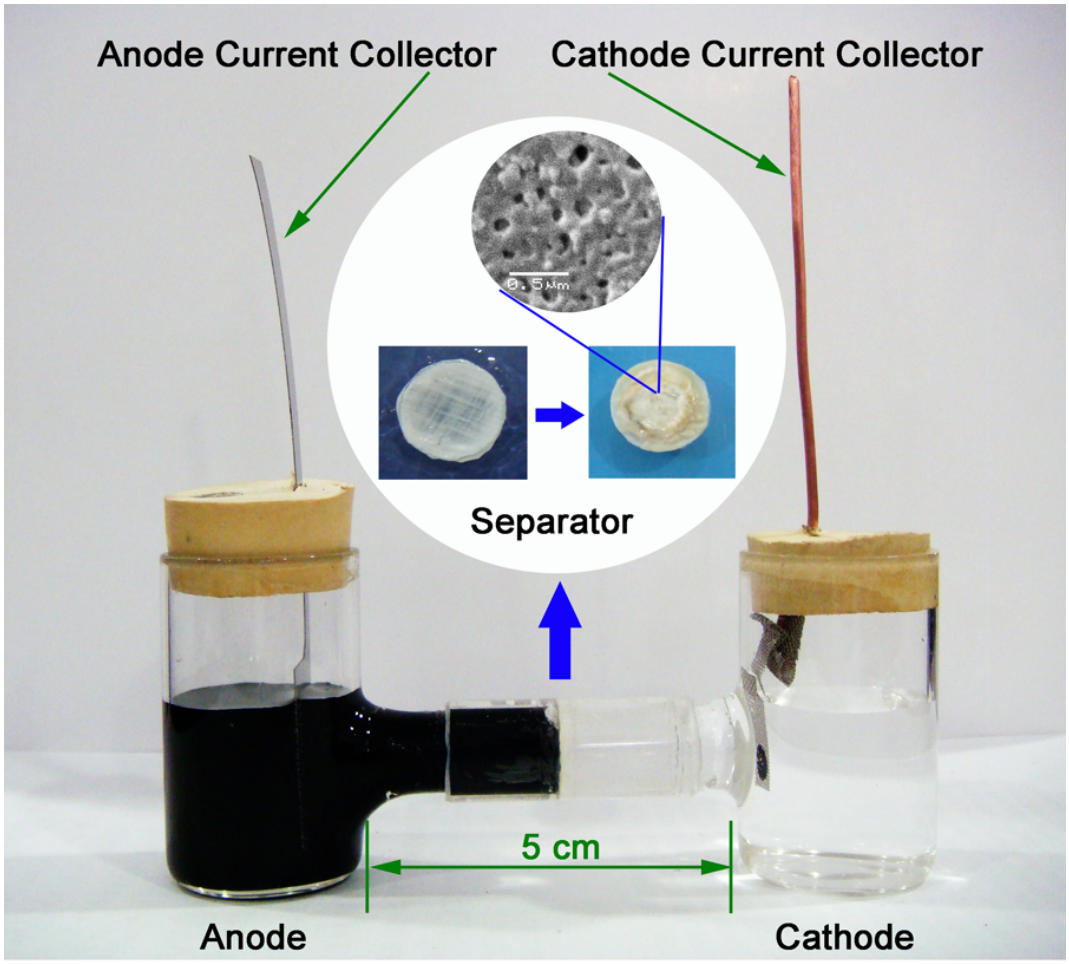

Fig. S2. The construction of the cell. The inset figure shows the changes of the separator before and after charge-discharge.

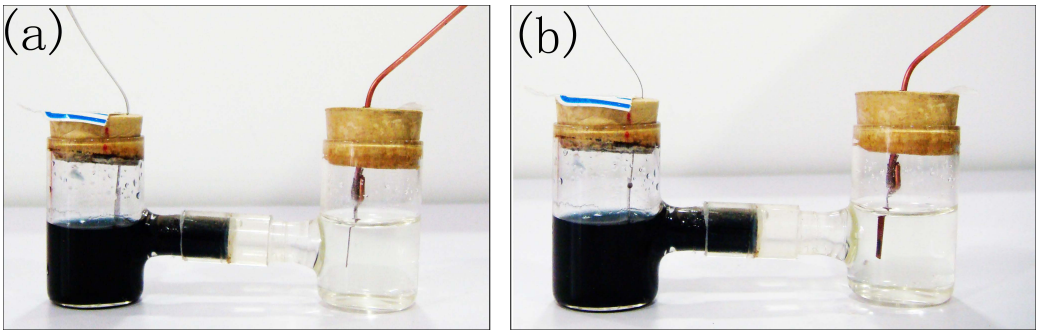

Fig. S3. Photos of the Cr^{3+}(aqueous)/$LiMn_2O_4$ HRFB in the presence of the sandwiched membrane with a distance of 6 cm between the current collector of the negative electrode and the positive electrode: (a) before cycling and (b) after 30 cycles at 110 mA g^{-1} (based on the mass of the positive material) followed by a storage for 3 months.

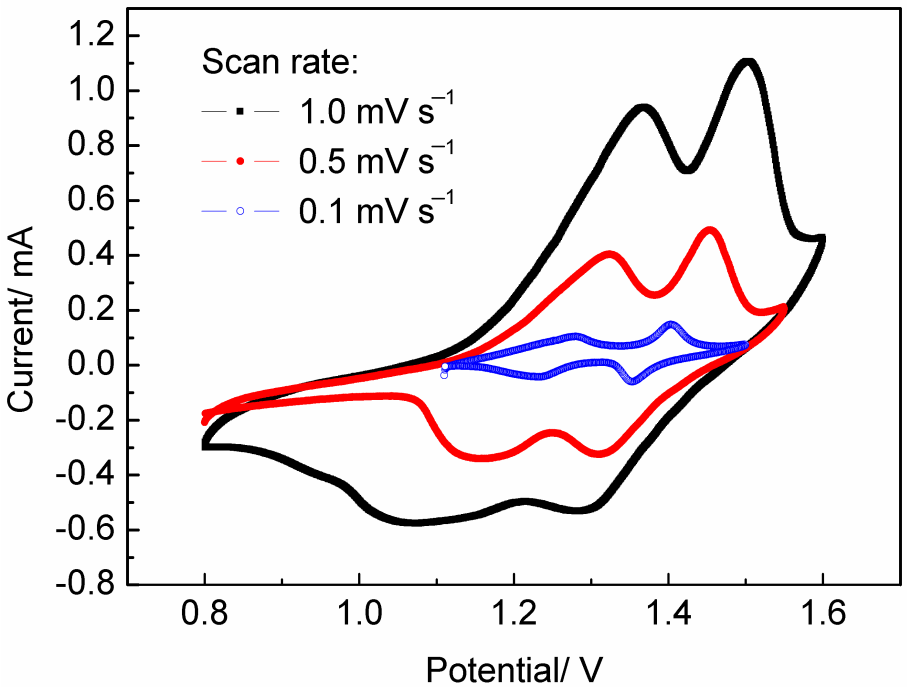

Fig. S4. Cyclic voltammograms of the hybrid redox flow battery (HRFB) consisting of 1 mol L^{-1} aqueous Cr^{3+} solution as the counter and reference electrode, solid $LiMn_2O_4$ as the work electrode, and the PVDF/PMMA-$LiClO_4$/PVDF sandwiched membrane as the separator at the scan rates of 0.1, 0.5 and 1.0 mV s^{-1}.

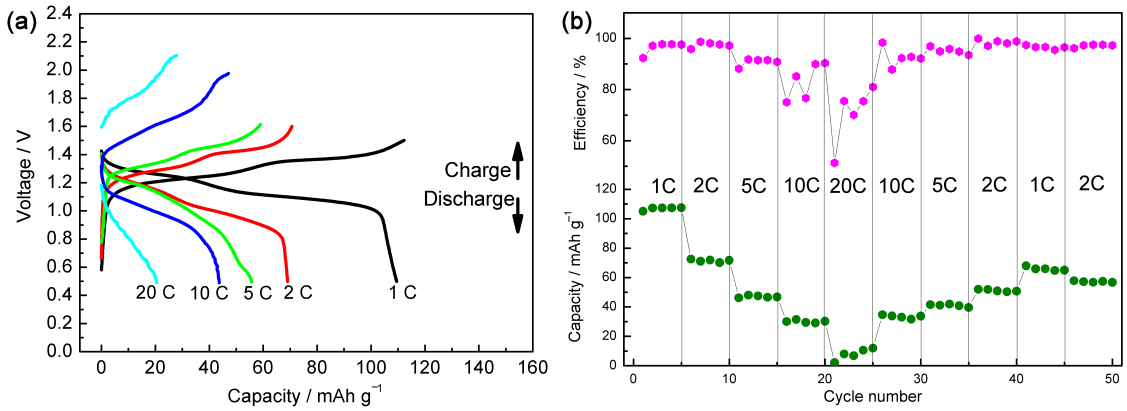

Fig. S5. Rate performances of the HRFB system based on the mass of $LiMn_2O_4$. (a) Charge-discharge curves and (b) capacity and efficiency recovery at various current densities.

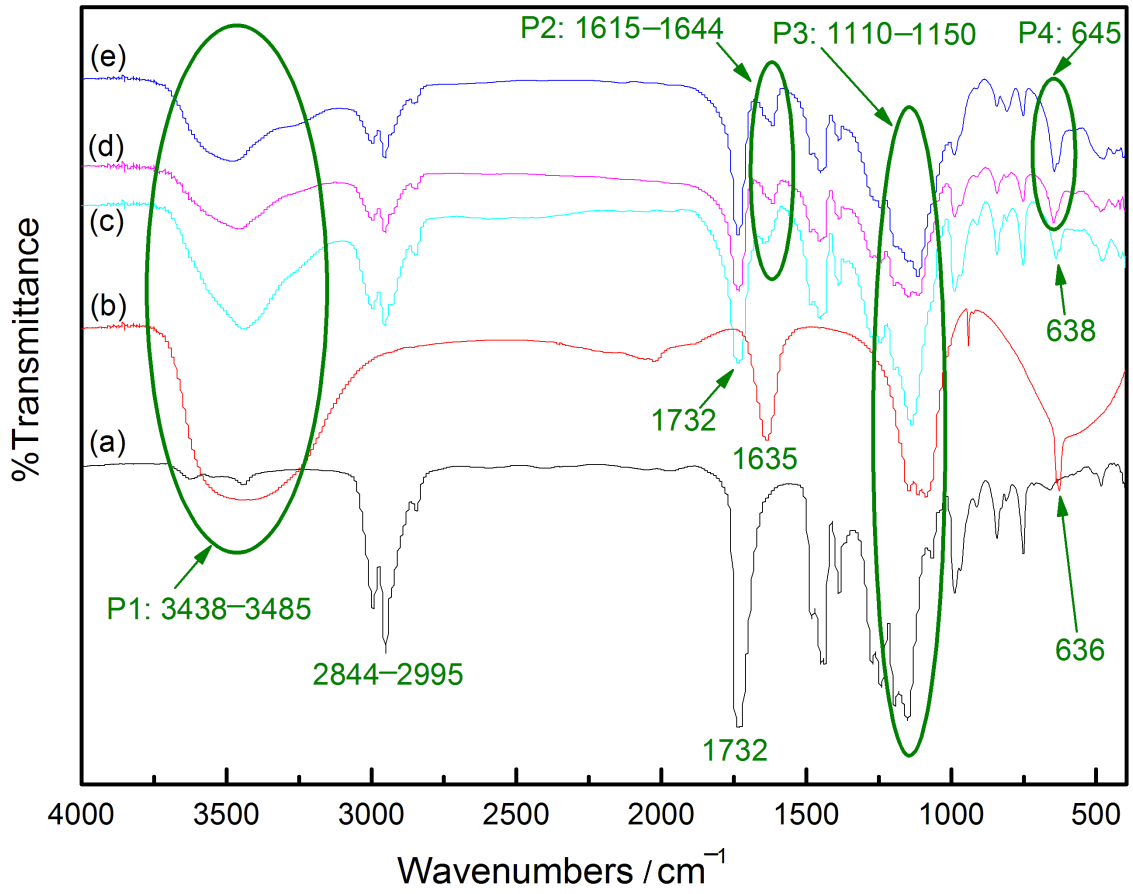

Fig. S6. FTIR of the samples. (a) Pure PMMA, (b) pure $LiClO_4$, (c) original PMMA-$LiClO_4$ film, and the peeled-off inner layer of the separator (d) after 30 cycles and (e) after 3 months.

Fig. S6 (a) and (b) presents a transmittance of pure PMMA and pure $LiClO_4$, respectively. The transmittances of curve (c), (d) and (e) are basically in agreement with (a)+(b) except for four peaks. Peak 1 (P1) located in the range of 3438–3485 cm^{-1} shows the symmetric-antisymmetric stretching vibration of –OH in crystal water in the bulk of $LiClO_4$. And P2 at 1615–1644 cm^{-1} is the bending vibration of H–O–H. Both P1 and P2 indicate the existence of water, which is understandable since $LiClO_4$ is hydrophilic. P3 located at 1110–1150 is somewhat complex. For curve (a), the pure PMMA, this region belongs to C–O–C stretching vibration located at 1149.3 and 1242 cm^{-1} with split peaks at 1193 cm^{-1} and 1272.9 cm^{-1}, respectively, which is the characteristic vibration peaks for simple homopolymer PMMA phase. In the case of curve (b), the pure $LiClO_4$, P3 region includes three split peaks located at 1087.8, 1112.9 and 1145.5 cm^{-1}, respectively, which is the ν_3 stretching vibration of the ionic ClO_4^{-1} group. In the case of curve (c), the original film of the separator, the corresponding peaks in this region move and change obviously. The peaks locate at 1135.2 and 1243.5 cm^{-1}, respectively, indicating that ClO_4^{-1} group

interacts closely with C–O–C because the character peaks move obviously. In the case of curve (d), the peeled-off inner layer of the separator after 30 cycles, the corresponding peaks locate at 1110.8 and 1243.7 cm^{-1}, respectively. Considering the lithium ion exchange between the inner layer and the electrolyte, the peak for ClO_4^{-1} group moves noticeably before and after using. And in the case of curve (e), the same movement is observed indicating that there are no obvious changes and the inner PMMA-$LiClO_4$ layer keeps stable after 3 months. P4 locates at 636 cm^{-1} is the ν_4 stretching vibration of the ionic ClO_4^{-1} group. After fabrication as shown in curve (c), the peak moves to 638 cm^{-1}. After 30 cycles and 3 months, as shown in curve (d) and (e), the peak locates at 645 cm^{-1}. This movement is in agreement with ν_3, which validates the stability of the inner layer further.

Table S1. ICP-AES results for ions in the HRFB system in discharged state.

	Ion concentrations in negative side ($g\ L^{-1}$)			Ion concentrations in positive side ($g\ L^{-1}$)		
	Original	After 30 cycles	After 3 months	Original	After 30 cycles	After 3 months
Li	19.926	20.078	20.065	20.027	20.034	20.028
Cr	102.533	102.539	102.528	0.003	0.007	0.007
Mn	0.001	0.001	0.001	0.001	0.001	0.001

Table S1 indicates that the ion concentration of each kind of ion remains stable when the HRFB system recovers after discharge, and the ionic selective separator is effective to block Cr ions passing through. The concentration of Mn element is ascribed to test error.

Table S2. Technology Comparison of Potential Batteries[a] for Utility Applications[b]

type	open circuit voltage (V)	specific energy ($W\ h\ kg^{-1}$)	operating temperature (°C)	Discharge time (h)	self-discharge % per month, @ 20 °C	cycle life (deep cycles)	round-trip DC energy efficiency (%)
LAB	2.1	25–40	–40–60	Up to 8 h	4–50	1000	50–75
NCB	1.35	30–45	–10–45	Up to 4 h	5–20	2000	55–70
VRB	1.4	10–20	10–40	4–12 h	3–9	5000	65–80
LCB	2.1	25–40	–40–60	Up to 4 h		3000	
Na-S	2.1	150–240	300–350	4–8 h	negligible	4000	75–90
ZEBRA	2.6	95–120	300–350	4–8 h	negligible	3000	75–90
C-LC	3–4	155	–25–40	Up to 4 h	2	1000	94–99
LTLFP	1.7	50–70	–25–40	Up to 4h	2	4000	94–99
CLB	1.4	30–45	–10–45	Up to 4 h	3–9	4000	85–95

[a] LAB: lead-acid batteries; NCB: nickel-cadmium batteries; VRB: all-vanadium redox flow batteries; LCB: lead-carbon ultrabatteries; Na-S: sodium-sulfur batteries; ZEBRA: Zeolite Battery Research Africa; C-LC: Li-ion batteries of C anode and $LiCoO_2$ cathode; LT-LFP: Li-ion batteries of $Li_4Ti_5O_{12}$ anode and $LiFePO_4$ cathode; CLB: Cr^{3+} (aqueous)/$LiMn_2O_4$ hybrid redox flow battery.

[b] Except CLB, the other data is referenced from dx.doi.org/10.1021/cr100290v |*Chem. Rev.* 2011, 111, 3577–3613.

Calculation of the theoretical energy density of the hybrid redox flow battery (with the ideal concentration of 100 wt% for the anode, ie, water is neglected at the state of 100% DOD)

(a) The HRFB system of $Cr_2(SO_4)_3/LiMn_2O_4$

$2LiMn_2O_4 + Cr_2(SO_4)_3 \rightarrow Li_2SO_4 + 2CrSO_4 + 4MnO_2$

$W = V \times 1000 / (Q^+ + Q^-)$ (W h kg^{-1})

Where W, V, Q^+ and Q^- represents energy density, open-circuit voltage, electrochemical equivalence of the cathode and electrochemical equivalence of the anode, respectively.

For this system, the V is 1.4 V.

$Q^+ = M_{LiMn_2O_4} / 26.8 = 180.82 / 26.8 = 6.75$ g $(A\ h)^{-1}$

$Q^- = M_{Cr_2(SO_4)_3} / (26.8 \times 2) = 392.18 / (26.8 \times 2) = 7.32$ g $(A\ h)^{-1}$

As a result, $W = 1.4 \times 1000 / (6.75 + 7.32) = 100$ W h kg^{-1}.

(b) The HRFB system of $CrCl_3//LiMn_2O_4$

According to the above calculation of (a), the energy density of this system can be calculated as the follows:

$Q^+ = M_{LiMn_2O_4} / 26.8 = 180.82 / 26.8 = 6.75$ g $(A\ h)^{-1}$

$Q^- = M_{CrCl_3} / 26.8 = 158 / 26.8 = 5.90$ g $(A\ h)^{-1}$

As a result, $W = 1.4 \times 1000 / (6.75 + 5.90) = 111$ W h kg^{-1}.

Calculation of the expected energy density of the hybrid redox flow battery (with a concentration of 30 wt% for the anode, ie, water is included)

$Q^+ = M_{LiMn_2O_4} / 26.8 = 180.82 / 26.8 = 6.75$ g $(A\ h)^{-1}$

$Q^- = M_{Cr_2(SO_4)_3} / (26.8 \times 2 \times 30\%) = 392.18 / (26.8 \times 2 \times 30\%) = 24.39$ g $(A\ h)^{-1}$

As a result, $W = 1.4 \times 1000 / (6.75 + 24.39) = 45$ W h kg^{-1}.

Calculation of the expected volumetric energy density of the hybrid redox flow battery (with a concentration of 30 wt% for the anode, ie, water is included, at the state of 100% DOD)

$W = U / (V^+ + V^-)$ (W h L^{-1})

Where W, U, V^+ and V^- represents volumetric energy density, open-circuit voltage, volumetric electrochemical equivalence of the cathode and volumetric electrochemical equivalence of the anode, respectively. For this system, the U is 1.4 V.

$V^+ = Q^+ / D_t^+ = 6.75/1.9 = 3.55$ cm^3 $(Ah)^{-1} = 3.55 \times 10^{-3}$ L $(Ah)^{-1}$

$V^- = Q^- / D_t^- = 24.39/1.47 = 16.59$ cm^3 $(Ah)^{-1} = 1.66 \times 10^{-2}$ L $(Ah)^{-1}$

Where D is the tap density of $LiMn_2O_4$, and D_t^- is the density of the 30 wt% $Cr_2(SO_4)_3$ mixed with 15 wt% Li_2SO_4 at room temperature.

Then W=69.5 W h L^{-1}

For comparison, the energy density of V flow battery is calculated in the same way

$2VOSO_4 + V_2(SO_4)_3 + 2H_2O \rightarrow (VO_2)_2SO_4 + 2VSO_4 + 2H_2SO_4$

(1) With a concentration of 100 wt% for both of the anode and the cathode (water participates the cathode reaction)

V=1.26 V

$Q_1^+ = M_{VOSO_4} / 26.8 = 163.00 / 26.8 = 6.08$ g $(A\ h)^{-1}$

$Q_2^+ = M_{H_2O} / 26.8 = 18.00 / 26.8 = 0.67$ g $(A\ h)^{-1}$

$Q^- = M_{V_2(SO_4)_3} / (26.8 \times 2) = 390.07 / (26.8 \times 2) = 7.28$ g $(A\ h)^{-1}$

As a result, $W = 1.26 \times 1000 / (6.08 + 0.67 + 7.28) = 90$ W h kg^{-1}.

(2) With a concentration of 30 wt% for both of the anode and the cathode (water

participates the cathode reaction and is included)

$Q_1^+ = M_{VOSO_4} / (26.8 \times 30\%) = 163.00 /(26.8 \times 30\%) = 20.27$ g $(A\ h)^{-1}$

$Q_2^+ = M_{H_2O} / 26.8 = 18.00 /26.8 = 0.67$ g $(A\ h)^{-1}$

$Q^- = M_{V_2(SO_4)_3} / (26.8 \times 2 \times 30\%) = 390.07 /(26.8 \times 2 \times 30\%) = 24.26$ g $(A\ h)^{-1}$

As a result, $W = 1.26 \times 1000 / (20.27 + 0.67 + 24.26) = 28$ W h kg^{-1}.

Calculation of the rated power density of the hybrid redox flow battery

$P=IV/\sum M$

where P, I, V and M represents the rated power density, working current, out-put voltage and the mass equivalence of the cathode and the anode, respectively.

$M^+ = M_{LiMn_2O_4} / (\eta 26.8) = 180.82/(0.75 \times 26.8) = 9.00$ g $(A\ h)^{-1}$

$M^- = M_{Cr_2(SO_4)_3} / (\eta 26.8 \times 2 \times wt\%) = 392.18/(1 \times 26.8 \times 2 \times 30\%) = 24.39$ g $(A\ h)^{-1}$

$\sum M=9.00+24.39=33.39$ A g^{-1}

where η is the discharge-charge efficiency.

I=1 A

V=1.15 V

As a result, $P = 1.15 \times 1 \times 1000 /33.39 = 34$ W kg^{-1}.

Table S3. The cell voltage components (50% state of charge, 298 K)

Parameter	Symbol	Value
Voltage of the cell, V	E_{cell}	1.154
Ohmic drop across the membrane, V	$I_m R_m$	8.06×10^{-3}
Ohmic drop associated with anolyte, V	$I_i R_i$	5.196×10^{-3}
Cathodic overpotential, V	η_p	0.01
Anodic overpotential, V	η_n	0.084
Ohmic drop associated with catholyte, V	$I_i R_i$	1.66×10^{-3}
Sum of the kinetic overpotentials, V	η	0.109

Equations employed for the calculated cell voltage components[1–10]

$$E_{cell} = E_{cell}^{rev} - I_m R_m - I_i R_i - \eta \qquad [1]$$

$$E_{cell}^{rev} = E_p^0 - E_n^0 \qquad [2]$$

Membrane ohmic drop

$$I_m R_m = I_m \frac{L_m}{\sigma_m} \qquad [3]$$

$$\sigma_m = (0.5139\lambda - 0.326)\exp\left(1268\left[\frac{1}{303} - \frac{1}{T}\right]\right) \qquad [4]$$

Anolyte ohmic drop

$$I_i R_i = 2 I_i \frac{L_x}{\kappa_n} \qquad [5]$$

$$\kappa_n = \frac{F^2}{RT} \sum_i z_i^2 D_i c_i^{\text{avg}} \qquad [6]$$

Catholyte ohmic drop[1, 2]

$$I_i R_i = 2 I_i \frac{L_x}{\kappa^{eff}} \qquad [7]$$

$$\kappa^{eff} = \frac{\kappa\varepsilon}{\tau} \qquad [8]$$

$$\tau = \gamma\varepsilon^{1-\alpha} \qquad [9]$$

$$\varepsilon = \frac{\rho_R - \rho_A}{\rho_R} \qquad [10]$$

Negative electrode overpotential

$$i_0 = F k_n^0 \; c_{\mathrm{O}}^{*(1-\beta)} \; c_{\mathrm{R}}^{*\beta} \qquad [11]$$

$$i = i_0 \left(\frac{c_{\mathrm{R}}(0,t)}{c_{\mathrm{R}}^*} \right) \exp\left(\frac{(1-\beta)F}{RT} \eta_n \right) \qquad [12]$$

Positive electrode overpotential

$$\eta_p = \frac{2RT}{F} \operatorname{asinh}\left(\frac{I}{2Fk_p \varepsilon a L_x \sqrt{c_{\mathrm{LiMn_2O_4}}^{\mathrm{s,avg}} c_{\mathrm{Li_{1-x}Mn_2O_4}}^{\mathrm{s,avg}}}} \right) \qquad [13]$$

$$k_p = k_p^0 \exp\left(\frac{FE_p^0}{R} \left[\frac{1}{T_{ref}} - \frac{1}{T} \right] \right) \qquad [14]$$

Table S4. Physical properties used in the above equations

Parameter	Symbol	Value	Ref.
Reversible equilibrium potential of the positive electrode, V	E_p^0	0.85	1
Reversible equilibrium potential of the negative electrode, V	E_n^0	–0.41	2
Constant associated with water content	λ	0.63	3,4
Diffusion coefficient of Cr^{2+} in electrolyte, $m^2\ s^{-1}$	$D(Cr^{2+})$	2.5×10^{-10}	5
Diffusion coefficient of Cr^{3+} in electrolyte, $m^2\ s^{-1}$	$D(Cr^{3+})$	1.78×10^{-9}	6
Diffusion coefficient of Li^+ in electrolyte, $m^2\ s^{-1}$	$D(Li^+)$	1.03×10^{-9}	6
Diffusion coefficient of SO_4^{2-} in electrolyte, $m^2\ s^{-1}$	$D(SO_4^{2-})$	2.13×10^{-9}	6
Tortuosity of a system	τ	0.5	3,7
Pre Bruggeman factor	γ	2	3,7
Bruggeman's value	α	1.5	3,7
Porosity of the positive electrode	ε	0.667	8
Standard rate constant, $m\ s^{-1}$	k_n^0	2×10^{-6}	9
Transfer coefficient (or the symmetry factor in transition state theory)	β	0.5	9
Reference rate constant for positive electrode (298 K), $m\ s^{-1}$	k_p^0	1.7×10^{-9}	10
Specific surface area, $m^2\ m^{-3}$	a	1.2×10^4	11[a]

[a]Conservative estimate based on literature and tested data.

References

1. Y. Cui, Z. Yuan, W. Bao, Q. Zhuang amd Z. Sun, *J. Appl. Electrochem.*, 2012, **42**, 883–891.
2. A. Z. Weber, M. M. Mench, J. P. Meyers, P. N. Ross, J. T. Gostick amd Q. Liu, *J. Appl. Electrochem.*, 2011, **41**, 1137–1164.
3. D. Stephenson, S. Kim, F. Chen, E. Thomsen, V. Viswanathan, W. Wang and V. Sprenkle, *J. Electrochem. Soc.*, 2012, **159**, A1993–A2000.
4. T. E. Springer, T. A. Zawodzinski and S. Gottesfeld, *J. Electrochem. Soc.*, 1991, **138**, 2334–2342.
5. P. Modiba, M. Matoetoe amd A. M. Crouch, *Electrochim. Acta*, 2013, **94**, 336–343.

6. D. R. Lide, *Handbook of Chemistry and Physics*, 84 ed. 2003, USA: CRC Press Inc.
7. E. Deiss, D. Häringer, P. Novák and O. Haas, *Electrochim. Acta*, 2001, **46**, 4185–4196.
8. W. Tang, S. Tian, L. L. Liu, L. Li, H. P. Zhang, Y. B. Yue, Y. Bai, Y. P. Wu and K. Zhu, *Electrochem. Commun*., 2011, **13**, 205–208.
9. A. Z. Weber, M. M. Mench, J. P. Meyers, P. N. Ross, J. T. Gostick amd Q. Liu, *J. Appl. Electrochem.*, 2011, **41**, 1137–1164.
10. H. Kanoh, Q. Feng, Y. Miyai and K. Ooi, *J. Electrochem. Soc.*, 1995, **142**, 702–707.
11. F. K. Shokoohi, J. M. Tarascon, B. J. Wilkens, D. Guyomard and C. C. Chang, *J. Electrochem. Soc.*, 1992, 139, 1845–1849.

Table S5. The performances in terms of figures of merit[12–14]

Performances	definition	Symbol	Value, %
Voltage efficiency	the ratio of cell voltage between discharge and charge cycles	η_V	96.6
Charge efficiency	the ratio of electrical charge used during discharge compared to that used during charge	η_C	98.3
Energy efficiency	the ratio of energy between the discharge and charge processes	η_E	90.2
Power efficiency	the ratio of power between discharge and charge processes	η_P	95.0

References

12. C. Ponce-de-León, G. W. Reade, I. Whyte, S. E. Male and F. C. Walsh, *Electrochim. Acta*, 2007, **52**, 5815–5823.
13. P. K. Leung, X. Li, C. Ponce de Léon, L. Berlouis, C. T. J. Low and F. C. Walsh, *RSC Advances,* 2012, **2**, 10125–10156.
14. C. Ponce-de-León, A. Frías-Ferrer, J. González-García, D. A. Szánto and F. C. Walsh, *J. Power Sources*, 2006, **160**, 716–732.